Structure *14*, 1003–1009, June 2006 DOI 10.1016/j.str.2006.04.007

Structure of a Central Component of the Yeast Kinetochore: The Spc24p/Spc25p Globular Domain

Ronnie R. Wei,[1,2] Jason R. Schnell,[1] Nicholas A. Larsen,[1] Peter K. Sorger,[3] James J. Chou,[1] and Stephen C. Harrison[1,2,*]

[1] Department of Biological Chemistry and Molecular Pharmacology
[2] Howard Hughes Medical Institute
Harvard Medical School
Boston, Massachusetts 02115
[3] Department of Biology and Biological Engineering Division
Massachusetts Institute of Technology
Cambridge, Massachusetts 02139

Summary

The Ndc80 complex, a kinetochore component conserved from yeast to humans, is essential for proper chromosome alignment and segregation during mitosis. It is an ~570 Å long, rod-shaped assembly of four proteins—Ndc80p (Hec1), Nuf2p, Spc24p, and Spc25p—with globular regions at either end of a central shaft. The complex bridges from the centromere-proximal inner kinetochore layer at its Spc24/Spc25 globular end to the microtubule binding outer kinetochore layer at its Ndc80/Nuf2 globular end. We report the atomic structures of the Spc24/Spc25 globular domain, determined both by X-ray crystallography at 1.9 Å resolution and by NMR. Spc24 and Spc25 fold tightly together into a single globular entity with pseudo-2-fold symmetry. Conserved residues line a common hydrophobic core and the bottom of a cleft, indicating that the functional orthologs from other eukaryotes will have the same structure and suggesting a docking site for components of the inner kinetochore.

Introduction

Kinetochores assemble on centromeric DNA, and during cell division they mediate bipolar attachment of chromosomes to spindle microtubules (MT). These attachments are stable during phases of microtubule polymerization and depolymerization, and they generate forces involved in metaphase and anaphase chromosome movement (Koshland et al., 1988). Kinetochores also regulate cell-cycle progression at the metaphase-to-anaphase transition through the spindle assembly checkpoint (Cleveland et al., 2003). Kinetochores carry out these crucial functions through concerted interactions among many proteins and protein complexes. In higher eukaryotes, electron microscopy of kinetochores reveals a trilaminar structure, with an electron-dense inner domain containing centromeric heterochromatin, a less dense middle domain, and an outer domain containing microtubule binding activities (Roos, 1973).

*Correspondence: schadmin@crystal.harvard.edu

Kinetochores in the budding yeast, *Saccharomyces cerevisiae,* assemble on a particularly simple centromere (*CEN*s). Short 125 bp point *CEN*s are sufficient for accurate chromosome segregation in *S. cerevisiae*, whereas the regional centromeres found in human cells span megabases of DNA, and those in fission yeast 100 kB or more (Chikashige et al., 1989; Clarke and Carbon, 1980; Cottarel et al., 1989). Kinetochores in higher eukaryotes bind 30 or more microtubules; those of budding yeast, a single MT (McDonald et al., 1992; Peterson and Ris, 1976; Winey et al., 1995). *S. cerevisiae* kinetochores are, nonetheless, large protein assemblies containing 60 or more different subunits organized into at least 14 multiprotein complexes (McAinsh et al., 2003). Moreover, sequence analysis of kinetochore proteins from various species reveals that many *S. cerevisiae* kinetochore proteins have been conserved from yeast to humans (Meraldi et al., 2006).

The four-protein Ndc80 kinetochore complex contains one copy of each of four essential proteins: Ndc80p, Nuf2p, Spc24p, and Spc25p. Close homologs of these proteins are found in all eukaryotes (Bharadwaj et al., 2004; Howe et al., 2001; McCleland et al., 2004; Wigge and Kilmartin, 2001; Zheng et al., 1999). Inactivation of Ndc80 complex proteins causes chromosomes to detach from spindle microtubules and thereby disrupts chromosome congression and segregation in all the fungi and metazoa studied. When the Ndc80 complex is depleted, checkpoint proteins such as Mad1 and Mad2 no longer target kinetochores or do so at much reduced levels (reviewd by Kline-Smith et al., 2005). Imaging of the Ndc80 complex in HeLa cells shows that hsNdc80 and hsNuf2 are present at the outer plate as stable components throughout mitosis, in contrast with the more dynamic distribution of motor and checkpoint proteins. hsNdc80 and hsNuf2 are essential for maintaining the integrity of the outer plate and thus for establishing stable kinetochore-microtubule attachment and tension (Deluca et al., 2005). In yeast, the Ndc80 complex requires CBF3 for localization at *CEN*s. Ndc80 in turn is needed for stable association of outer kinetochore proteins in various eukaryotes, including Stu2 and Dam1 in yeast (He et al., 2001; Janke et al., 2002; Li et al., 2005) and Zw10 in *Xenopus* (McCleland et al., 2003). The complex thus appears to link MT binding and checkpoint proteins to structures such as CBF3 that contact centromeric (*CEN*) DNA.

We recently reported reconstitution of the *S. cerevisiae* Ndc80 complex from recombinant proteins and analysis of its structure by biochemical methods and electron microscopy (Wei et al., 2005). Similar studies of the homologous human complex show a conserved structural organization (Ciferri et al., 2005). The Ndc80 complex appears to be a long rod with globular "heads" at either end of an α-helical coiled-coil shaft. Ndc80p and Nuf2p contribute to one head and to the intervening shaft; Spc24p and Spc25p complete the shaft and contribute to the other head (Figure 1). This molecular organization is appropriate for the postulated role of the complex as a connector between microtubule binding

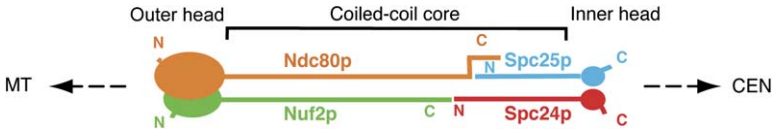

Figure 1. Schematic Diagram of the Ndc80 Complex

MT, microtubule; CEN, centromere. Each subunit is represented by an oval (the globular domain) and a stick (the coiled-coil region). The coiled-coils of Ndc80p/Nuf2p and Spc24p/Spc25p form the shaft. The globular domains of Ndc80p/Nuf2p form the "outer" head, which faces the microtubule; the globular domains of the Spc24p/Spc25p, the "inner" head, which faces the centromere.

proteins and DNA binding proteins (De Wulf et al., 2003). The stiff linkage between Ndc80p/Nuf2p and Spc24p/Spc25p subcomplexes would allow it to maintain tension between spindle and chromosome. Spc24p and Spc25p are both required for localization of Ndc80p and Nuf2p at kinetochores, but the reverse requirement is not observed (Bharadwaj et al., 2004; Gillett et al., 2004). It thus appears that the Spc24p/Spc25p end of the complex points to the centromere, and the Ndc80/Nuf2 end to the microtubule. The full complex is of suitable length to span the middle domain of a trilaminar kinetochore and to project the Spc24p/Spc25p end toward the inner plate.

High-resolution structures of several checkpoint proteins have been determined (Larsen and Harrison, 2004; Sironi et al., 2002; Sessa et al., 2005), but none for any core kinetochore component. We report here the atomic structure of the carboxy-terminal regions of *S. cerevisiae* Spc24p/Spc25p and establish that these two segments form an integrated globular domain. The most conserved residues lie at the dimer interface, and we conclude that the folded structure we describe is conserved in other organisms, despite low sequence identity among the functional orthologs. A groove on the surface that faces away from the coiled-coil shaft is a likely binding site for inner kinetochore proteins.

Results and Discussion

In our previous analysis of the yeast Ndc80 complex, we characterized a protease-resistant heterodimer of the Spc24p and Spc25p globular C-terminal domains—Spc24G (residues 138–213) and Spc25G (residues 128–221). (We use the residue numbers corresponding to the native, full-length yeast protein sequences throughout this report; where necessary, we add 24 or 25 in parentheses after a number to identify the subunit). We first determined the structure of this globular heterodimer by NMR spectroscopy (Table 1). The line widths and the absence of [^{15}N,^{1}H] NOEs for resonances from residues 138–154 of Spc24p and 128–132 of Spc25p indicated that these segments were disordered. We then expressed two shorter chains, with the disordered segments removed, and determined the crystal structure of the heterodimer by multiwavelength anomalous diffraction (MAD) from a Se-Met derivatized crystal at a resolution of 1.9 Å (Table 2). The final model contains residues 155–213 of Spc24p and 133–221 of Spc25p.

The NMR and crystal structures are very similar (Figure 2A). The Spc24G and Spc25G chains have the same fold—an antiparallel β sheet sandwiched between two helices (Figures 2B and 2C)—and the heterodimer has pseudo-2-fold symmetry. The complex has the overall shape of a butterfly, with a short, coiled-coil-like helical element as antennae, two laterally disposed β sheets as wings, and C-terminal helices as the body. The Spc25 "wing" has an additional strand and helix inserted between β3 and α2. A search (with DALI; Holm and Sander, 1993) of all known structures in the Protein Data Bank did not reveal any structural homologs for Spc24G, Spc25G, or the heterodimer.

Differences between the NMR solution structure and the crystal structure are mainly in the loops connecting

Table 1. NMR Structural Statistics and Atomic Rms Differences[a]

Quantity	Number of Restraints	Violations per Structure
NOEs	681	0.25 ± 0.55 (>0.2 Å)
Intramolecular	165/467	
Intermolecular	49	
Dihedral angle restraints	34	0
χ^a	10/13	0
χ^b	11/0	0
Dipolar coupling restraints (Hz)[b]	173	2.55 ± 0.12
NH	50/62	2.05 ± 0.11
$C'C^\alpha$	0/61	3.30 ± 0.19
Other restraints		
H-bond	26/38	0.45 ± 0.69 (>0.1 Å)
ϕ/ψ	58/115	0.2 ± 0.41 (>2.5°)
Deviations from idealized covalent geometry		
Bonds (Å)	0.0030 ± 0.0001	
Angles (deg)	0.44 ± 0.01	
Impropers (deg)	0.39 ± 0.01	
Coordinate precision (Å)[c]		
All heavy atoms	1.55	
Backbone heavy atoms	1.05	
Ramachandran plot statistics (%)[d]		
Most favored regions	78.8/79.7	
Additional allowed regions	14.2/14.6	
Generously allowed regions	6.3/4.6	
Disallowed regions	0.7/1.1	

[a] Statistics are calculated and averaged over the 20 structures with the lowest overall energy. Numbers are reported for the combined dimer or the individual monomers (Spc24/Spc25).

[b] Violations are given as the rms difference (in Hz) between individual sets of experimental dipolar couplings, and those predicted by the 20 final structures by means of SVD fit. The $^{1}D_{C'C\alpha}$ couplings are normalized to $^{1}D_{NH}$.

[c] The precision of the atomic coordinates is defined as the average rms difference between the 20 final structures and their mean coordinates.

[d] As evaluated with the program PROCHECK (Laskowski et al., 1993).

Table 2. Crystallographic Statistics

	MAD λ1	*MAD λ2*	*MAD λ3*
Data collection			
Wavelength (Å)	0.9795	0.97970	0.95370
Space group	$I4_122$	$I4_122$	$I4_122$
Resolution[a] (Å)	50.00-1.90 (1.97-1.90)	50.00-1.90 (1.97-1.90)	50.00-1.90 (1.97-1.90)
Unique observations	13,743	13,820	13,711
Redundancy[a]	17.8 (12.9)	17.9 (12.6)	9.6 (7.0)
Completeness[a] (%)	99.8 (97.9)	99.5 (94.7)	99.5 (94.9)
$I/\sigma(I)$[a]	33.4 (7.4)	37.1 (7.0)	29.6 (5.4)
R_{sym}[b]	0.082	0.078	0.068
Refinement			
Resolution (Å)			20.0-1.9
No. of refined protein residues			149
No. of refined solvent atoms			126
R_{cryst}[c]			0.209
R_{free}[d]			0.226
Average B-factor Spc25/Spc24/water (Å^2)			24.5/23.0/33.5
Bond length rmsd (Å)			0.017
Angle rmsd (°)			1.55
Ramachandran plot (% in most favored/allowed/generous/disallowed regions)			93.2/6.8/0/0

[a] Numbers in parenthesis refer to the highest resolution shell.
[b] $R_{merge} = \sum_{ij}|(I_i(j) - <I(j)>| / \sum_{ij} I_i(j)$, where $I_i(j)$ is the intensity of the i-th observation of reflection j. I(j) is the weighted mean of all measurements of j.
[c] $R_{cryst} = \sum_j| F_o(j)| - |F_c(j)| / \sum_j|F_o(j)|$, where F_o and F_c are the observed and calculated structure factors.
[d] R_{free} was calculated as for R_{cryst} but on 5% of data excluded before refinement.

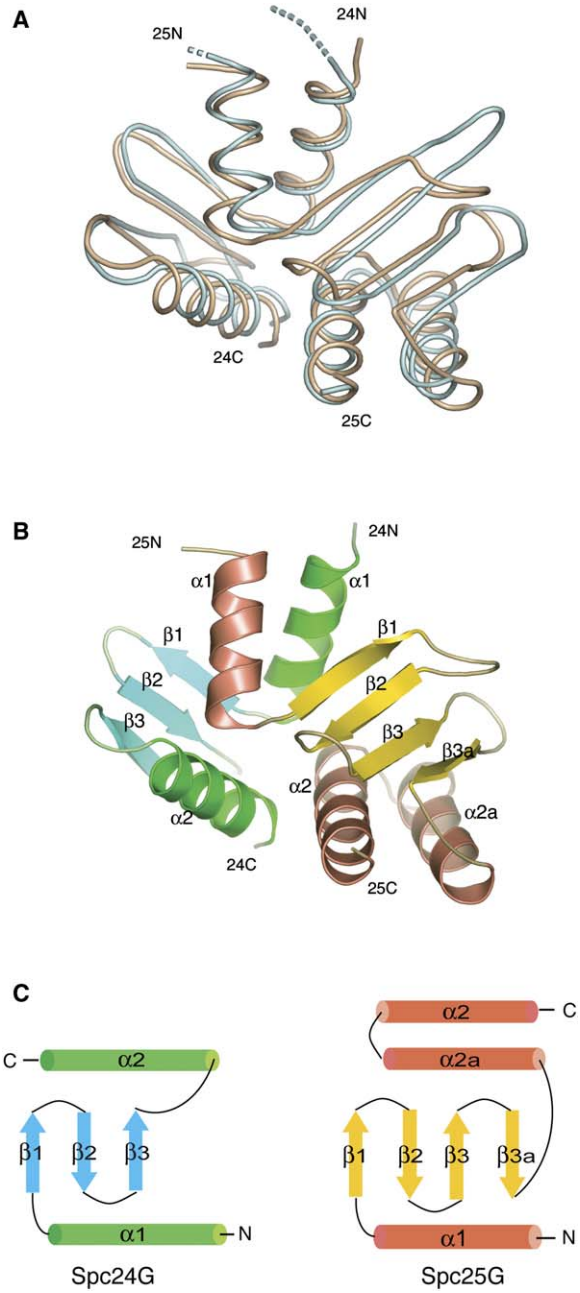

Figure 2. Overview of the NMR and Crystal Structures of Spc24G/Spc25G

(A) Superposition of the backbones of the solution NMR structure (light blue) and crystal structure (gold). The dotted lines represent unstructured residues 138–154 of Spc24G and 128–132 of Spc25G. The N and C termini of Spc24G and Spc25G are labeled with " 24N," "24C," "25N," and "25C," respectively.

(B) Ribbon diagram of the crystal structure in the same view as in (A). The α helices and β strands are orange and yellow in Spc24G and green and blue in Spc25G, respectively.

(C) Folding diagram of Spc24G and Spc25G. The secondary structures are colored as in (B). The N and C termini are labeled with "N" and "C," respectively.

the β strands of Spc25G. NMR signals from the backbone amides of residues in the β1-β2, β2-β3, and β3-β3a loops of Spc25G are missing or are very weak and exhibit few interresidue NOEs, suggesting high flexibility. The same residues exhibit high crystallographic B factors in the crystal structure (data not shown). We conclude that these loops are intrinsically flexible.

Spc24G and Spc25G associate very stably, even without the long coiled-coil regions at the N-terminal ends of the two intact proteins (Wei et al., 2005). Their interface buries 2464 Å^2 of molecular surface, an unusually large area for a relatively small dimer (~17 kDa). Thus, it is reasonable to think of the two subunits as folded together into a single globular domain, with conserved Trp208(24) at the center of its hydrophobic core, surrounded by seven leucines and two phenylalanines from both subunits. In addition, Thr204(24) from α2 forms the C-cap for α1 of Spc25G, and R214 from α2 of Spc25G forms an NH-π interaction with the indole ring of Trp208(24) (Figure 3B). A [^{15}N,^{1}H] HSQC spectrum from Spc25G alone indicates that Spc25G is partially unfolded in the absence of Spc24G (data not shown). The structure also explains previous observations in human cells that RNAi of Spc24 abolishes kinetochore targeting of Spc25 and vice versa (McCleland et al., 2004).

The "head-rod-head" architecture of Ndc80 has been conserved from yeast to man. Like their budding yeast counterparts, hsSpc24p and hsSpc25p have coiled-coil segments at their N termini, followed by globular regions (Ciferri et al., 2005). The amino acid sequences of the human and yeast Spc24p and Spc25p correspond only weakly, with overall 14% and 12% identity and

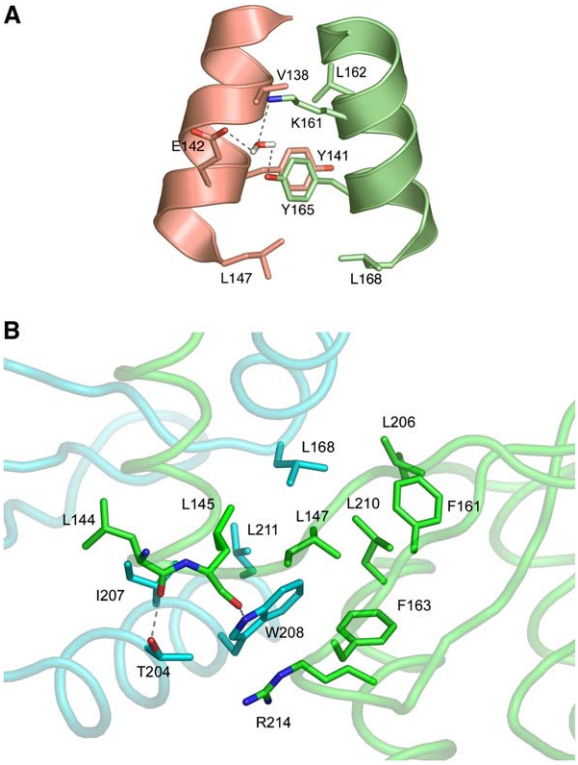

Figure 3. The Dimer Interface of Spc24G/Spc25G

(A) The coiled-coil interaction of the α1 helices, showing the side chains at their interface. Carbons are in green in α1 of Spc24G and in orange in α1 of Spc25G. Oxygen and nitrogen atoms are in red and blue, respectively. Hydrogen bonds are shown as gray dotted lines. A water molecule links E142(25) with K161(24) and Y165(24) in a hydrogen-bond network.

(B) The hydrophobic core, with contribution from both subunits. The polypeptide backbones are shown as tubes (Spc24G, blue; Sc25G, green). The side chains of participating residues and the carbonyls of L144(25) and L145(25) are shown in stick representation.

28% and 23% similarity, respectively. We compared the sequences of Spc24G and Spc25G from several species of fungi and metazoa (Figure 4) and mapped the conserved residues onto the structure (Figure 5). Most of the strongly conserved residues cluster along the dimer interface (Figure 5), indicating that dimer integrity has been maintained during evolution and further leading us to conclude that the 2SG module from other eukaryotes has a structure similar to the one described here.

The segments that link the N-terminal coiled-coils of Spc24p and Spc25p with the globular elements in our structure correspond to residues 126–157 and 117–133, respectively. The amino acid sequences of these segments are quite divergent (not shown), relatively rich in Pro and Gly, and very low in coiled-coil propensity (Paircoil; Berger et al., 1995). Our NMR spectra also show that residues 138–157 (24) and 128–133 (25) are disordered, even when they extend from the folded, globular heterodimer. We therefore believe that these segments are a flexible joint between the rod-like part of the Spc24p/25p heterodimer and its globular head.

No direct binding partners for Spc24p/Spc25p have yet been identified despite the importance of the Ndc80 complex in linking inner and outer kinetochore components. The structural interdependence of Spc24p and Spc25p shows why no search with only one of the two subunits as the "bait" could have worked for finding a potential "prey." A marked groove in the Spc24G/Spc25G dimer faces away from the short coiled-coil formed by the two α1 helices. Trp208(24) lies at the base of this groove, buttressed by three of the remaining four residues fully conserved among the sequences in Figure 4 (see Figures 5A and 5B). Moreover, a conserved hydrophobic patch on α2 of Spc24G, including Ser199, Phe201, Tyr202, and Tyr206, faces the groove (Figures 5B and 6), and Tyr206 is one of the residues mutated in a temperature-sensitive allele of *spc24* (Wigge and Kilmartin, 2001). Within the range of flexibility imparted by the connecting segments described in the preceding paragraph, the groove in the 2SG dimer would project away from the shaft of the Ndc80 complex. The groove thus has all the properties we might expect for a site of interaction with a partner protein, possibly a component of the inner kinetochore, such as CBF3, Mif2, or Cse4.

Experimental Procedures

Sample Preparation

The solution structural sample composed of Spc25G (128–221) and Spc24G (138–213) with a cleavable hexa-histidine tag was overexpressed in Rosetta pLyS cells (Novagen) induced by 1 mM IPTG and purified by affinity and size-exclusion chromatography. Spc25G (133–221) and Spc24G (154–213) were expressed and purified in the same way as the NMR samples, with the exception that the selenomethionyl protein derivatives were expressed in the methionine auxotroph cell line BL834(DE3) (Novagen). Selenomethionine incorporation was confirmed by mass spectrometry.

Samples for NMR experiments were isotopically labeled by growing cells in M9 media substituted with one or more of the following: ^{15}N-labeled ammonium chloride, ^{13}C-labeled glucose, and 99% D_2O. The unlabeled component was prepared in Luria-Bertani medium (see X-ray section). NMR samples were prepared in 260 μl 95% H_2O/5% D_2O with 280 μl Shigemi microcells. Final NMR samples contained 1–2 mM protein, 20 mM potassium phosphate, and 1 mM azide at pH 7.0. Residual dipolar couplings (RDCs) were collected on a sample that was weakly aligned in the magnet by adding 15 mg/ml of the filamentous phage Pf1 (ASLA Biotech).

NMR Measurements

All NMR spectra were collected at 30ºC on a Bruker spectrometer operating at a ^{1}H frequency of 600 MHz and equipped with a cryogenic probe. Except where noted, all spectra were collected twice on mixed dimers in which only one component was isotopically labeled. Resonance assignments were obtained from a suite of triple-resonance experiments as described previously (Oxenoid and Chou, 2005). Distance restraints were obtained from ^{15}N-NOESY spectra with mixing times of 100 and 120 ms (Spc24) or 120 ms (Spc25) and a ^{13}C-NOESY spectra with a mixing time of 150 ms. Intermolecular distance restraints were obtained from a ^{15}N-edited, double-^{13}C-filtered NOESY spectra (Oxenoid and Chou, 2005; Zwahlen et al., 1997) with a mixing time of 120 ms (Spc24) or 160 ms (Spc25). Side-chain χ_1 (Spc24 and Spc25) and χ_2 (Spc24 only) rotamers of methyl-bearing residues and χ_1 of aromatic residues were obtained from three bond coupling constants as described (Oxenoid and Chou, 2005). Backbone amide dipolar couplings ($^1D_{NH}$) were measured (Ikura et al., 1990; Kontaxis et al., 2000) with 50 ms of mixed CT ^{15}N evolution. In addition, ^{13}C′-^{13}C$^{\alpha}$ couplings ($^1D_{C'C\alpha}$) were measured for the Spc25-labeled dimer by a quantitative *J* method (Jaroniec et al., 2004). All NMR data processing was done in NMRPipe (Delaglio et al., 1995) and analyzed in CARA (Keller, 2004) or XEASY (Bartels et al., 1995).

NMR Structure Calculation

Refinement was performed with the program XPLOR-NIH (Schwieters et al., 2003). Initial rounds of high-temperature (800 K) simulated annealing were used to obtain the overall fold, followed by

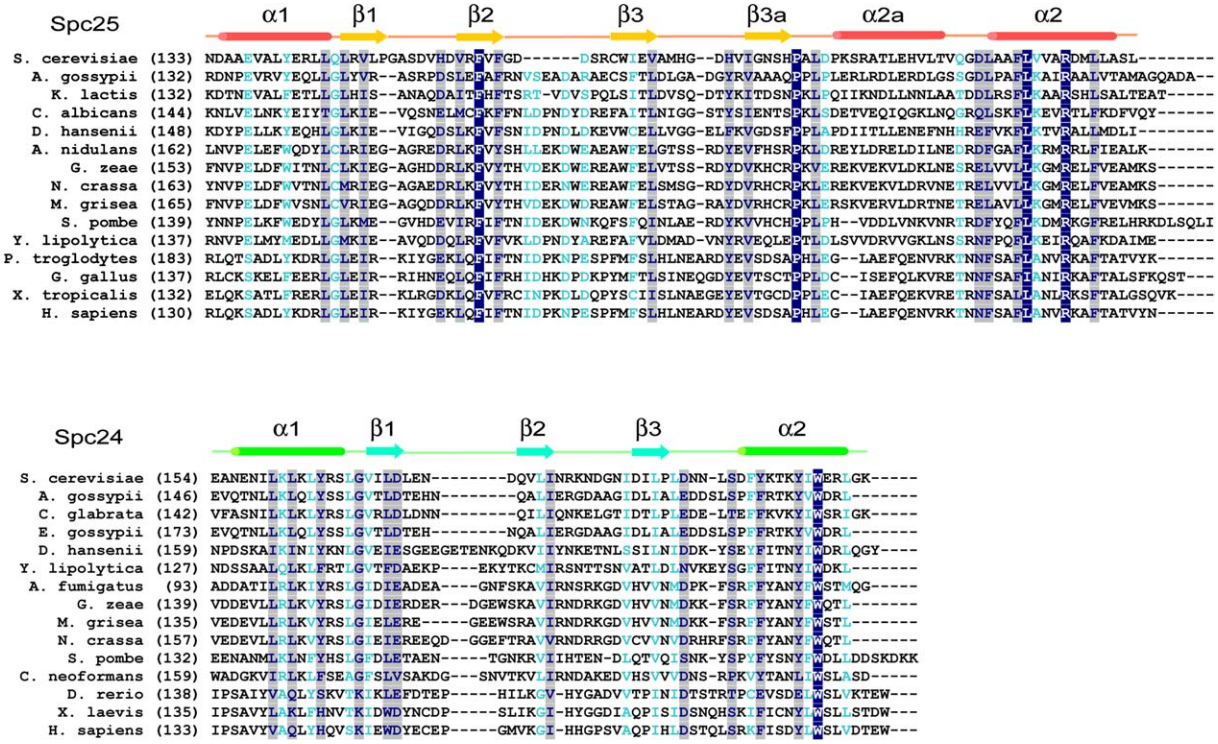

Figure 4. Multiple Sequence Alignment for Spc24G and Spc25G

Secondary structural elements derived from the crystal structure are colored following the same scheme as in Figure 2B. The starting residue number for each homolog is specified in parentheses after the species name. The alignment was generated with CLUSTAL W (Chenna et al., 2003). Residues are colored according to their degree of conservation. Identical residues are in white letters on a dark blue background. Strongly conserved residues are in blue on a gray background and weakly conserved residues in lighter blue.

low-temperature (300 K) simulated annealing to optimize local geometry (Chou et al., 2000a, 2000b). Experimental data consisted of distance restraints from NOEs, side-chain χ_1 and χ_2 angles from $^3J_{NC\gamma}$, $^3J_{C'C\gamma}$, and $^3J_{C\gamma C\delta}$ scalar couplings, and relative bond angles from RDCs. Final distance and bond angle restraint force constants were 100 kcal mol^{-1} rad^{-2} and 0.075 kcal mol^{-1} Hz^{-2}, respectively. Side-chain rotamers were enforced as flat-well (±30°) harmonic potentials with force constants fixed at 20 kcal mol^{-1} rad^{-2}. In addition, hydrogen-bond distance restraints of 2 and 3 Å (O-H^N and O-N, respectively) were enforced for the rigid helical and β strand regions,

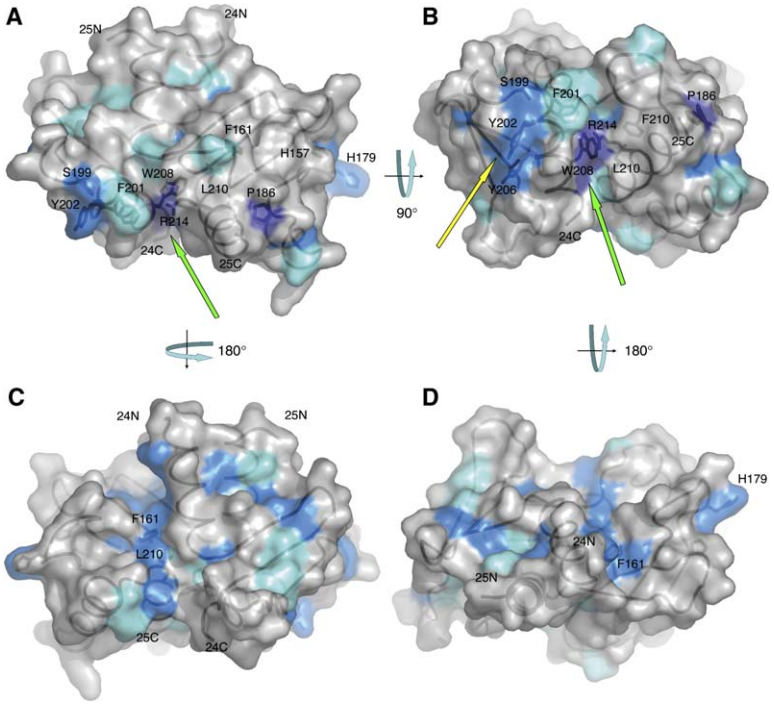

Figure 5. Surface Representation of Spc24G/Spc25G Showing Location of Conserved Residues on the Protein Surface

The protein is drawn as a transparent molecular surface with individual polypeptide backbones as tubes visible from within. Dark blue, blue, and light blue show strictly, strongly, and weakly conserved regions, respectively, in accordance with Figure 4. The side chains of strictly conserved residues and relatively highly conserved residues are shown as sticks. The termini of the two subunits are labeled when visible. (A) View as in Figure 2. (B) View from below in (A), showing the C termini of the dimer. Next to the conserved central groove surrounding W208 (24) is a conserved, exposed, hydrophobic patch containing S199, F201, Y202, and Y206 of Spc24G. (C) View from the opposite direction of the one in (A), showing conserved patches along the dimer interface. (D) View from the opposite direction of the one in (B). The green arrows point to the conserved groove, and the yellow arrow points to the conserved hydrophobic patch.

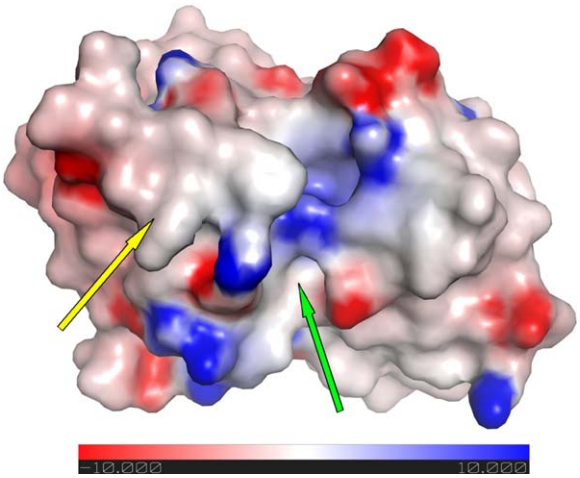

Figure 6. Surface Representation of Spc24G/Spc25G Showing Electrostatic Potential

View as in Figure 5B. Red and blue surfaces correspond to negative and positive electrostatic potential scaled from $-10\ k_bT$ to $10\ k_bT$, respectively. The green arrows point to the conserved groove, and the yellow arrow points to the conserved hydrophobic patch as in Figure 5B.

with flat-well (±0.2 Å) harmonic potentials, and force constants of 20 kcal mol^{-1} $Å^{-2}$. A weak database-derived "Rama" potential function (Kuszewski et al., 1997) was ramped from 0.02 to 0.2 (dimensionless force constant) for the general treatment of side-chain rotamers. From the calculation of 30 structures, 20 were chosen based on overall energy to represent the ensemble (see the Supplemental Data available with this article online). Refinement statistics of the 20 final structures are given in Table 1. Coordinates have been deposited in the PDB with access code 2FV4.

Structure Determination by Crystallography

Proteins were concentrated to 15 mg/ml in 20 mM bis-tris propane (pH 7.6), 250 mM NaCl, 10 mM DTT, and crystallized by hanging drop vapor diffusion against a reservoir solution of 0.1 M CAPS (pH 10.5), 1.2 M NaH_2PO_4/0.8 M K_2HPO_4, 0.2 M Li_2SO_4. Crystals were transferred to the reservoir solution containing 18% (v/v) glycerol before flash freezing in liquid nitrogen. MAD data were collected at the Advanced Light Source beamline 8.2.2 and processed with HKL2000 (Otwinowski and Minor, 1997). Crystals belong to space group $I4_122$ with cell dimensions a = b = 84.92 Å, c = 92.74 Å, and one Spc25G/Spc24G heterodimer per asymmetric unit with a solvent content of 46.4%. Positions of three out of four total selenium sites were located with SOLVE (Terwilliger and Berendzen, 1999). Density modification and initial model building was performed with RESOLVE (Terwilliger, 2000), with an FOM of 0.77. Iterative manual model building was carried out with O (Jones et al., 1991) and Coot (Emsley and Cowtan, 2004), coupled with refinement by using Refmac5 (Murshudov et al., 1997). Data collection and refinement statistics are listed in Table 2. Coordinates have been deposited in the PDB with access code 2FTX.

Supplemental Data

Supplemental Data include one figure and are available at http://www.structure.org/cgi/content/full/14/6/1003/DC1/.

Acknowledgments

The authors thank Anna Wang for technical help, Kim Simons for sharing his knowledge and enthusiasm, Piotr Sliz for computational assistance, and Viji Draviam for critical review of the manuscript. We would like to acknowledge the Advanced Light Source at Lawrence Berkeley National Laboratory and the Center for Magnet Resonance at Massachusetts Institute of Technology (National Institutes of Health grant number EB002026). P.K.S. is supported by National Institutes of Health grant GM51464. N.A.L. acknowledges a postdoctoral fellowship from the Jane Coffin Childs Memorial Fund for Medical Research. J.J.C. is the recipient of the Smith Family Award for Young Investigators and the Pew scholarship. S.C.H. is an investigator of the Howard Hughes Medical Institute.

Received: March 9, 2006
Revised: April 28, 2006
Accepted: April 28, 2006
Published: June 13, 2006

References

Bartels, C., Xia, T., Billeter, M., Guntert, P., and Wuthrich, K. (1995). The Program XEASY for computer-supported NMR spectral analysis of biological macromolecules. J. Biomol. NMR *6*, 1–10.

Berger, B., Wilson, D.B., Wolf, E., Tonchev, T., Milla, M., and Kim, P.S. (1995). Predicting coiled coils by use of pairwise residue correlations. Proc. Natl. Acad. Sci. USA *92*, 8259–8263.

Bharadwaj, R., Qi, W., and Yu, H. (2004). Identification of two novel components of the human NDC80 kinetochore complex. J. Biol. Chem. *279*, 13076–13085.

Chenna, R., Sugawara, H., Koike, T., Lopez, R., Gibson, T.J., Higgins, D.G., and Thompson, J.D. (2003). Multiple sequence alignment with the Clustal series of programs. Nucleic Acids Res. *31*, 3497–3500.

Chikashige, Y., Kinoshita, N., Nakaseko, Y., Matsumoto, T., Murakami, S., Niwa, O., and Yanagida, M. (1989). Composite motifs and repeat symmetry in *S. pombe* centromeres: direct analysis by integration of NotI restriction sites. Cell *57*, 739–751.

Chou, J.J., Delaglio, F., and Bax, A. (2000a). Measurement of one-bond 15N-13C′ dipolar couplings in medium sized proteins. J. Biomol. NMR *18*, 101–105.

Chou, J.J., Li, S., and Bax, A. (2000b). Study of conformational rearrangement and refinement of structural homology models by the use of heteronuclear dipolar couplings. J. Biomol. NMR *18*, 217–227.

Ciferri, C., De Luca, J., Monzani, S., Ferrari, K.J., Ristic, D., Wyman, C., Stark, H., Kilmartin, J., Salmon, E.D., and Musacchio, A. (2005). Architecture of the human ndc80-hec1 complex, a critical constituent of the outer kinetochore. J. Biol. Chem. *280*, 29088–29095.

Clarke, L., and Carbon, J. (1980). Isolation of the centromere-linked CDC10 gene by complementation in yeast. Proc. Natl. Acad. Sci. USA *77*, 2173–2177.

Cleveland, D.W., Mao, Y., and Sullivan, K.F. (2003). Centromeres and kinetochores: from epigenetics to mitotic checkpoint signaling. Cell *112*, 407–421.

Cottarel, G., Shero, J.H., Hieter, P., and Hegemann, J.H. (1989). A 125-base-pair CEN6 DNA fragment is sufficient for complete meiotic and mitotic centromere functions in *Saccharomyces cerevisiae*. Mol. Cell. Biol. *9*, 3342–3349.

De Wulf, P., McAinsh, A.D., and Sorger, P.K. (2003). Hierarchical assembly of the budding yeast kinetochore from multiple subcomplexes. Genes Dev. *17*, 2902–2921.

Delaglio, F., Grzesiek, S., Vuister, G.W., Zhu, G., Pfeifer, J., and Bax, A. (1995). NMRPipe: a multidimensional spectral processing system based on UNIX pipes. J. Biomol. NMR *6*, 277–293.

Deluca, J.G., Dong, Y., Hergert, P., Strauss, J., Hickey, J.M., Salmon, E.D., and McEwen, B.F. (2005). Hec1 and nuf2 are core components of the kinetochore outer plate essential for organizing microtubule attachment sites. Mol. Biol. Cell *16*, 519–531.

Emsley, P., and Cowtan, K. (2004). Coot: model-building tools for molecular graphics. Acta Crystallogr. D Biol. Crystallogr. *60*, 2126–2132.

Gillett, E.S., Espelin, C.W., and Sorger, P.K. (2004). Spindle checkpoint proteins and chromosome-microtubule attachment in budding yeast. J. Cell Biol. *164*, 535–546.

He, X., Rines, D.R., Espelin, C.W., and Sorger, P.K. (2001). Molecular analysis of kinetochore-microtubule attachment in budding yeast. Cell *106*, 195–206.

Holm, L., and Sander, C. (1993). Protein structure comparison by alignment of distance matrices. J. Mol. Biol. *233*, 123–138.

Howe, M., McDonald, K.L., Albertson, D.G., and Meyer, B.J. (2001). HIM-10 is required for kinetochore structure and function on *Caenorhabditis elegans* holocentric chromosomes. J. Cell Biol. *153*, 1227–1238.

Ikura, M., Kay, L.E., and Bax, A. (1990). A novel approach for sequential assignment of 1H, 13C, and 15N spectra of proteins: heteronuclear triple-resonance three-dimensional NMR spectroscopy. Application to calmodulin. Biochemistry *29*, 4659–4667.

Janke, C., Ortiz, J., Tanaka, T.U., Lechner, J., and Schiebel, E. (2002). Four new subunits of the Dam1-Duo1 complex reveal novel functions in sister kinetochore biorientation. EMBO J. *21*, 181–193.

Jaroniec, C.P., Ulmer, T.S., and Bax, A. (2004). Quantitative J correlation methods for the accurate measurement of 13C′-13Calpha dipolar couplings in proteins. J. Biomol. NMR *30*, 181–194.

Jones, T.A., Zou, J.Y., Cowan, S.W., and Kjeldgaard. (1991). Improved methods for building protein models in electron density maps and the location of errors in these models. Acta Crystallogr. A *47*, 110–119.

Keller, R. (2004). Optimizing the process of nuclear magnetic resonance spectrum analysis and computer aided resonance assignment. PhD thesis, Swiss Federal Institute of Technology, Zurich, Switzerland.

Kline-Smith, S.L., Sandall, S., and Desai, A. (2005). Kinetochore-spindle microtubule interactions during mitosis. Curr. Opin. Cell Biol. *17*, 35–65.

Kontaxis, G., Clore, G.M., and Bax, A. (2000). Evaluation of cross-correlation effects and measurement of one-bond couplings in proteins with short transverse relaxation times. J. Magn. Reson. *143*, 184–196.

Koshland, D.E., Mitchison, T.J., and Kirschner, M.W. (1988). Polewards chromosome movement driven by microtubule depolymerization in vitro. Nature *331*, 499–504.

Kuszewski, J., Gronenborn, A.M., and Clore, G.M. (1997). Improvements and extensions in the conformational database potential for the refinement of NMR and X-ray structures of proteins and nucleic acids. J. Magn. Reson. *125*, 171–177.

Larsen, N.A., and Harrison, S.C. (2004). Crystal structure of the spindle assembly checkpoint protein Bub3. J. Mol. Biol. *344*, 885–892.

Laskowski, R.A., MacArthur, M.W., Moss, D.S., and Thornton, J.M. (1993). PROCHECK: a program to check the stereochemical quality of protein structure. J. Appl. Crystallogr. *26*, 283–291.

Li, J.M., Li, Y., and Elledge, S.J. (2005). Genetic analysis of the kinetochore DASH complex reveals an antagonistic relationship with the ras/protein kinase A pathway and a novel subunit required for Ask1 association. Mol. Cell. Biol. *25*, 767–778.

McAinsh, A.D., Tytell, J.D., and Sorger, P.K. (2003). Structure, function, and regulation of budding yeast kinetochores. Annu. Rev. Cell Dev. Biol. *19*, 519–539.

McCleland, M.L., Gardner, R.D., Kallio, M.J., Daum, J.R., Gorbsky, G.J., Burke, D.J., and Stukenberg, P.T. (2003). The highly conserved Ndc80 complex is required for kinetochore assembly, chromosome congression, and spindle checkpoint activity. Genes Dev. *17*, 101–114.

McCleland, M.L., Kallio, M.J., Barrett-Wilt, G.A., Kestner, C.A., Shabanowitz, J., Hunt, D.F., Gorbsky, G.J., and Stukenberg, P.T. (2004). The Vertebrate Ndc80 Complex contains Spc24 and Spc25 homologs, which are required to establish and maintain kinetochore-microtubule attachment. Curr. Biol. *14*, 131–137.

McDonald, K.L., O'Toole, E.T., Mastronarde, D.N., and McIntosh, J.R. (1992). Kinetochore microtubules in PTK cells. J. Cell Biol. *118*, 369–383.

Meraldi, P., McAinsh, A.D., Rheinbay, E., and Sorger, P.K. (2006). Phylogenetic and structural analysis of centromeric DNA and kinetochore proteins. Genome Biol. *7*, R23.

Murshudov, G.N., Vagin, A.A., and Dodson, E.J. (1997). Refinement of macromolecular structures by the maximum-likelihood method. Acta Crystallogr. D Biol. Crystallogr. *53*, 240–255.

Otwinowski, Z., and Minor, W. (1997). Processing of X-ray diffraction data collected in oscillation mode. Methods Enzymol. *276*, 307–326.

Oxenoid, K., and Chou, J.J. (2005). The structure of phospholamban pentamer reveals a channel-like architecture in membranes. Proc. Natl. Acad. Sci. USA *102*, 10870–10875.

Peterson, J.B., and Ris, H. (1976). Electron-microscopic study of the spindle and chromosome movement in the yeast *Saccharomyces cerevisiae*. J. Cell Sci. *22*, 219–242.

Roos, U.P. (1973). Light and electron microscopy of rat kangaroo cells in mitosis. II. Kinetochore structure and function. Chromosoma *41*, 195–220.

Schwieters, C.D., Kuszewski, J.J., Tjandra, N., and Marius Clore, G. (2003). The Xplor-NIH NMR molecular structure determination package. J. Magn. Reson. *160*, 65–73.

Sessa, F., Mapelli, M., Ciferri, C., Tarricone, C., Areces, L.B., Schneider, T.R., Stukenberg, P.T., and Musacchio, A. (2005). Mechanism of Aurora B activation by INCENP and inhibition by hesperadin. Mol. Cell *18*, 379–391.

Sironi, L., Mapelli, M., Knapp, S., Antoni, A.D., Jeang, K.-T., and Musacchio, A. (2002). Crystal structure of the tetrameric Mad1-Mad2 core complex: implications of a 'safety belt' binding mechanism for the spindle checkpoint. EMBO J. *21*, 2496–2506.

Terwilliger, T. (2000). Maximum-likelihood density modification. Acta Crystallogr. D Biol. Crystallogr. *56*, 965–972.

Terwilliger, T.C., and Berendzen, J. (1999). Automated MAD and MIR structure solution. Acta Crystallogr. D Biol. Crystallogr. *55*, 849–861.

Wei, R.R., Sorger, P.K., and Harrison, S.C. (2005). Molecular organization of the Ndc80 complex, an essential kinetochore component. Proc. Natl. Acad. Sci. USA *102*, 5363–5367.

Wigge, P.A., and Kilmartin, J.V. (2001). The Ndc80p complex from *Saccharomyces cerevisiae* contains conserved centromere components and has a function in chromosome segregation. J. Cell Biol. *152*, 349–360.

Winey, M., Mamay, C.L., O'Toole, E.T., Mastronarde, D.N., Giddings, T.H., Jr., McDonald, K.L., and McIntosh, J.R. (1995). Three-dimensional ultrastructural analysis of the *Saccharomyces cerevisiae* mitotic spindle. J. Cell Biol. *129*, 1601–1615.

Zheng, L., Chen, Y., and Lee, W.H. (1999). Hec1p, an evolutionarily conserved coiled-coil protein, modulates chromosome segregation through interaction with SMC proteins. Mol. Cell. Biol. *19*, 5417–5428.

Zwahlen, C., Legault, P., Vincent, S.J.F., Greenblatt, J., Konrat, R., and Kay, L.E. (1997). Methods for measurement of intermolecular NOEs by multinuclear NMR spectroscopy: application to a bacteriophage N-peptide/boxB RNA complex. J. Am. Chem. Soc. *119*, 6711–6721.

Accession Numbers

The crystal and NMR solutions structures have been entered into the Protein Data Bank under the accession numbers 2FTX and 2FV4, respectively.